Stem Cell Reports
Report
ISSCR
OPEN ACCESS

De novo DNA methyltransferases DNMT3A and DNMT3B are essential for *XIST* silencing for erosion of dosage compensation in pluripotent stem cells

Atsushi Fukuda,[1,2,3,4,5,7,*] Dane Z. Hazelbaker,[2] Nami Motosugi,[3] Jin Hao,[1,2] Francesco Limone,[1,2] Amanda Beccard,[2] Patrizia Mazzucato,[2] Angelica Messana,[2] Chisa Okada,[6] Irune Guerra San Juan,[1,2] Menglu Qian,[1,2] Akihiro Umezawa,[7] Hidenori Akutsu,[7] Lindy E. Barrett,[1,2] and Kevin Eggan[1,2,*]

[1]The Harvard Stem Cell Institute and Department of Stem Cell and Regenerative Biology, Harvard University, Cambridge, MA, USA
[2]Stanley Center for Psychiatric Research, Broad Institute of MIT and Harvard, Cambridge, MA, USA
[3]Department of Molecular Life Science, Division of Basic Medical Science and Molecular Medicine, Tokai University School of Medicine, Isehara, Kanagawa, Japan
[4]The Institute of Medical Science, Tokai University, Kanagawa, Japan
[5]Micro/Nano Technology Center, Tokai University, Hiratsuka, Kanagawa, Japan
[6]Support Center for Medical Research and Education, Tokai University School of Medicine, Isehara, Kanagawa, Japan
[7]Center for Regenerative Medicine, National Center for Child Health and Development, Tokyo, Japan
*Correspondence: fa972942@tsc.u-tokai.ac.jp (A.F.), eggan@mcb.harvard.edu (K.E.)
https://doi.org/10.1016/j.stemcr.2021.07.015

SUMMARY

Human pluripotent stem cells (hPSCs) have proven to be valuable tools for both drug discovery and the development of cell-based therapies. However, the long non-coding RNA *XIST*, which is essential for the establishment and maintenance of X chromosome inactivation, is repressed during culture, thereby causing erosion of dosage compensation in female hPSCs. Here, we report that the *de novo* DNA methyltransferases DNMT3A/3B are necessary for *XIST* repression in female hPSCs. We found that the deletion of both genes, but not the individual genes, inhibited *XIST* silencing, maintained the heterochromatin mark of H3K27me3, and did not cause global overdosage in X-linked genes. Meanwhile, *DNMT3A/3B* deletion after *XIST* repression failed to restore X chromosome inactivation. Our findings revealed that *de novo* DNA methyltransferases are primary factors responsible for initiating erosion of dosage compensation in female hPSCs, and *XIST* silencing is stably maintained in a *de novo* DNA-methylation-independent manner.

INTRODUCTION

During female mammalian development, each cell selects one of the two X chromosomes for inactivation to achieve dosage compensation of gene expression (Augui et al., 2011). A key step in this process, known as X chromosome inactivation (XCI), is established through the expression of the long non-coding X-inactive specific transcript, *XIST* RNA (Augui et al., 2011). Genetic studies in mice have shown that *Xist* is essential for initiation (Marahrens et al., 1997) and normal maintenance of XCI (Csankovszki et al., 2001). However, in both female human induced pluripotent stem cells (iPSCs) and human embryonic stem cells (hESCs) cultured under standard "primed" conditions, the expression of *XIST* is routinely lost (Anguera et al., 2012; Mekhoubad et al., 2012; Patel et al., 2017; Sahakyan et al., 2018). Once *XIST* expression is silenced in a human pluripotent stem cell (hPSC), this state is propagated through subsequent cell divisions and is associated with a loss of the repressive H3K27me3 mark, overlapped with *XIST* RNA (Mekhoubad et al., 2012; Sahakyan et al., 2017; Vallot et al., 2015), as well as widespread changes in DNA CpG methylation (Mekhoubad et al., 2012; Patel et al., 2017; Vallot et al., 2015). Ultimately, these events result in the inappropriate, biallelic expression of X-linked genes and affect the differentiation potential (Mekhoubad et al., 2012; Salomonis et al., 2016; Vallot et al., 2015). These events, which have been dubbed "erosion" of dosage compensation, share many similarities with those occurring after conditional deletion of *Xist* from the mouse inactive X chromosome (Csankovszki et al., 2001; Marahrens et al., 1997).

While conversion to a naive state was suggested to potentially help correct *XIST* repression, the naive cell culture conditions currently known and used have limited ability to restore dosage compensation (Guo et al., 2017; Sahakyan et al., 2017) and may cause chromosomal abnormalities (Liu et al., 2017). Given these observations, it is essential to understand how *XIST* silencing, resulting in erosion of dosage compensation, is induced in hPSCs. An increased mechanistic understanding might in turn allow erosion to be prevented prior to the deployment of female hPSCs in both disease modeling and cell replacement therapies.

RESULTS

Inhibition of DNA methylation reactivates *XIST* during hPSC differentiation

It is well known that the *XIST* locus becomes methylated in male cells, which do not express *XIST*, and remains relatively unmethylated in female cells that do transcribe the RNA (Chapman et al., 2014). The findings from the study suggested that the *XIST*-expressing allele exhibits

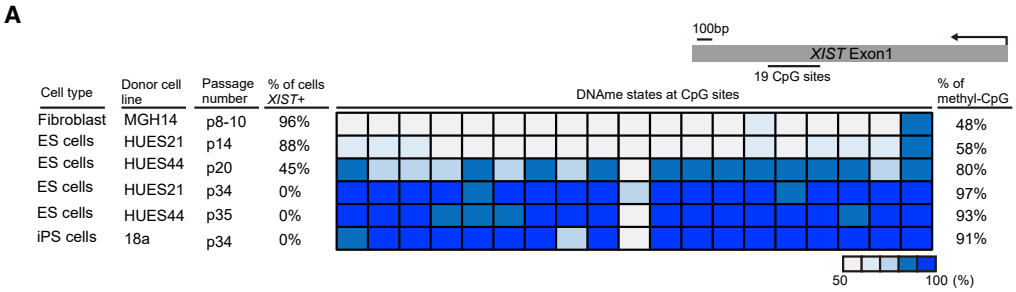

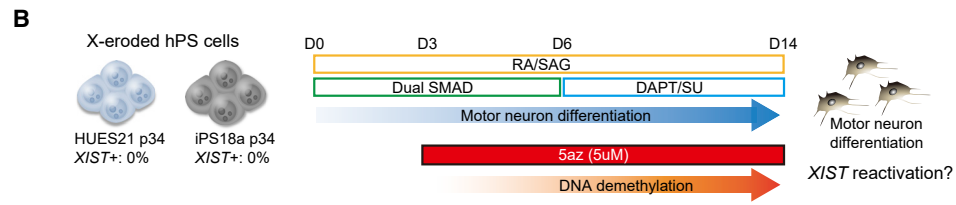

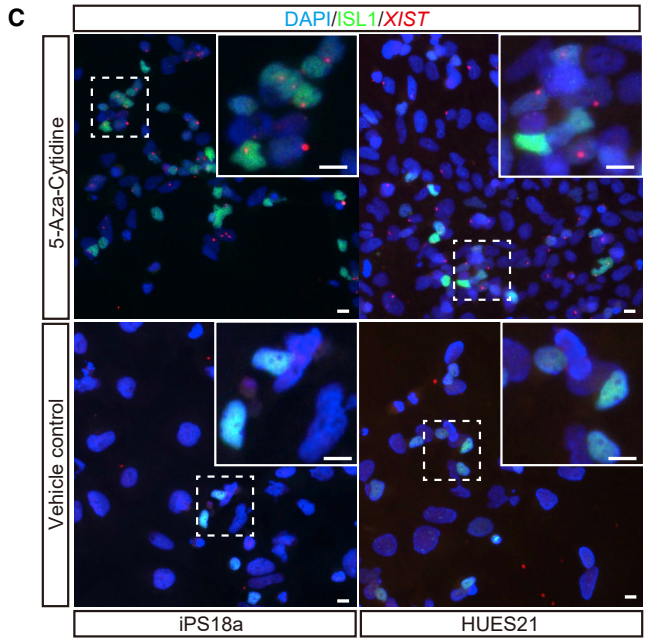

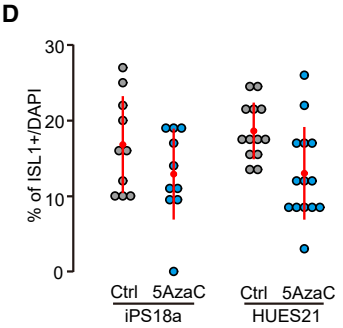

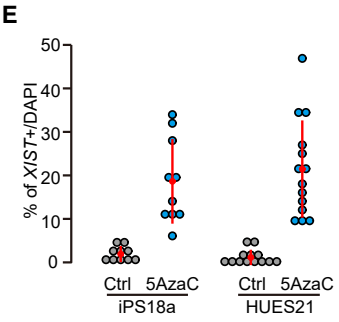

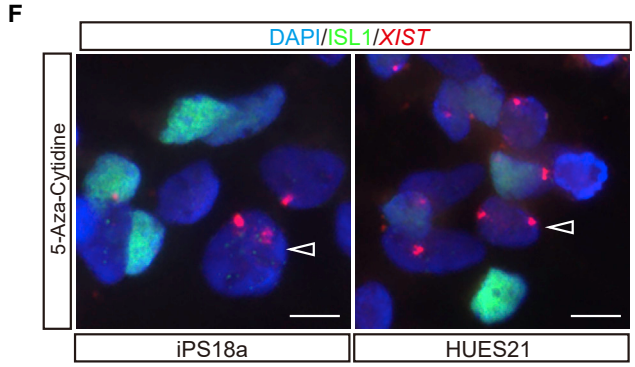

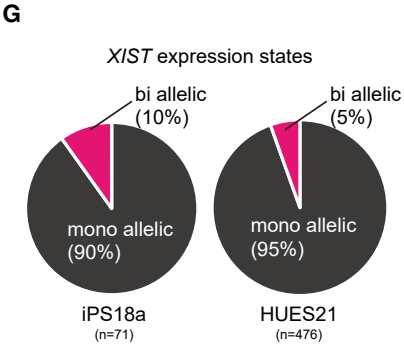

(legend on next page)

approximately 50% DNA methylation, whereas DNA is hypermethylated in cells without *XIST* expression. We previously reported that after erosion of dosage compensation, female hPSCs acquired increased levels of *XIST* methylation, which were similar to those observed in male cells (Mekhoubad et al., 2012). We began our studies by investigating the generality and reproducibility of changes in *XIST* DNA methylation using three different female hPSC lines with distinct passage numbers as well as a somatic cell control. This new analysis of *XIST* DNA methylation by bisulfite sequencing and transcript expression by fluorescence *in situ* hybridization (FISH) confirmed that reduced expression of *XIST* and the onset of erosion did indeed correlate with an increase in *XIST* DNA methylation (Figure 1A).

We next wondered whether these changes in methylation at the *XIST* promoter were merely correlated with *XIST* silencing or instead directly related to its functional repression. To test this idea we attempted to reduce DNA methylation levels in eroded hPSCs by using the DNA methyltransferase inhibitor 5-azacytidine (5azaC) (Christman, 2002). Unfortunately, treatment with 5azaC resulted in rapid hPSC death (Figure S1), consistent with a previous report suggesting that the activity of the maintenance methyltransferase DNMT1 is essential for hPSC self-renewal (Liao et al., 2015). It is also well known that the toxicity of 5azaC is most pronounced in rapidly dividing cells (Szyf, 2011). We therefore next wondered if 5azaC treatment during directed differentiation down the motor neuron lineage would allow cells to survive 5azaC treatment due to their slowing rates of cell division, while still undergoing sufficient DNA replication to enable passive demethylation (Figure 1B). To this end, we initiated a well-established motor neuron differentiation scheme with two eroded cell lines (iPSC 18a and hESC HUES21) and at day 3 of differentiation began administering 5azaC. After 11 additional days of differentiation with 5azaC administration, we quantified the number of ISL1-expressing spinal motor neurons and monitored *XIST* expression by RNA-FISH. As anticipated, the efficiency of motor neuron differentiation decreased in both 5azaC-treated cultures (Figures 1C and 1D), suggesting that 5azaC remained modestly toxic. Despite the negative effect on differentiation, 5azaC treatment led to a substantial and significant induction of *XIST* expression in both eroded cell lines (Figures 1C–1E). Interestingly, we also noted biallelic expression of *XIST* by FISH in a small portion of cells treated with 5azaC (Figures 1F and 1G). Overall, these initial results are consistent with the notion that DNA methylation is required in the differentiating derivatives of hPSCs to maintain silencing of *XIST* on both the active X chromosome and the "eroded" X chromosome following erosion of dosage compensation.

DNMT3A and DNMT3B are essential for *XIST* repression, resulting in erosion of dosage compensation

The *de novo* DNA methyltransferases *DNMT3A* and *DNMT3B* are expressed during pre- and post-preimplantation embryo development, where they mediate the establishment of lineage-specific DNA methylation patterns (Smith et al., 2014). However, we showed that upon explant of the human inner cell mass into culture conditions for hPSC derivation, an immediate and significant increase in genome-wide levels of DNA methylation occurred that was carried over into the resulting hESCs and that is also seen upon human iPSC reprogramming (Meissner, 2010). We wondered whether this increase in DNA methylation found previously might also be related to the accumulation of methylation at *XIST*. If so, we reasoned that elimination of one or both of the *de novo* DNA methyltransferases in hPSCs might prevent *XIST* silencing. To test this idea, we identified a culture of HUES21 that was largely composed of cells still harboring an inactive X (>80%) and then used CRISPR-Cas9 to generate mutant sub-clones harboring homozygous loss-of-function mutations in *DNTM3A* or *DNMT3B* alone, as well as clones with mutations in both of the *de novo* methyltransferases (Figure 2A). We then identified, by DNA sequencing and western blot analysis, appropriate wild type or mutant sub-clones and double mutants cloned that also retained an inactive X chromosome as measured by H3K27me3 staining (Figures 2A, 2B, S2A, and S2B).

Using the resulting mutant, double mutant, and control sub-clones, we performed continuous cell culture over 18 days and monitored the erosion of dosage compensation by measuring the expression of *XIST* and the X-active specific transcript (*XACT*), a marker of erosion (Vallot et al.,

Figure 1. DNA methylation suppresses *XIST* expression after erosion of dosage compensation

(A) Bisulfite sequence analysis at *XIST* in hPSCs and a somatic cell line. The percentage of *XIST* expression state was determined by RNA-FISH experiments.

(B) Experimental scheme for motor neuron differentiation with 5azaC.

(C) Immunofluorescence staining (ISL1) combined with *XIST* RNA-FISH at day 14. The scale bar represents 10 μm.

(D and E) Quantification of ISL1- (D) and *XIST*-positive (E) cells relative to DAPI in iPS18a and HUES21 p34. Each dot indicates the percentage of ISL- or *XIST*-positive cells in the observed area in two independent experiments. In each group, >424 cells were analyzed.

(F and G) Immunofluorescence staining (F) and quantification (G) of cells with *XIST* mono- and biallelic expression. The arrowheads indicate cells with biallelic *XIST* expression. The scale bar represents 10 μm. n means the number of cells analyzed.

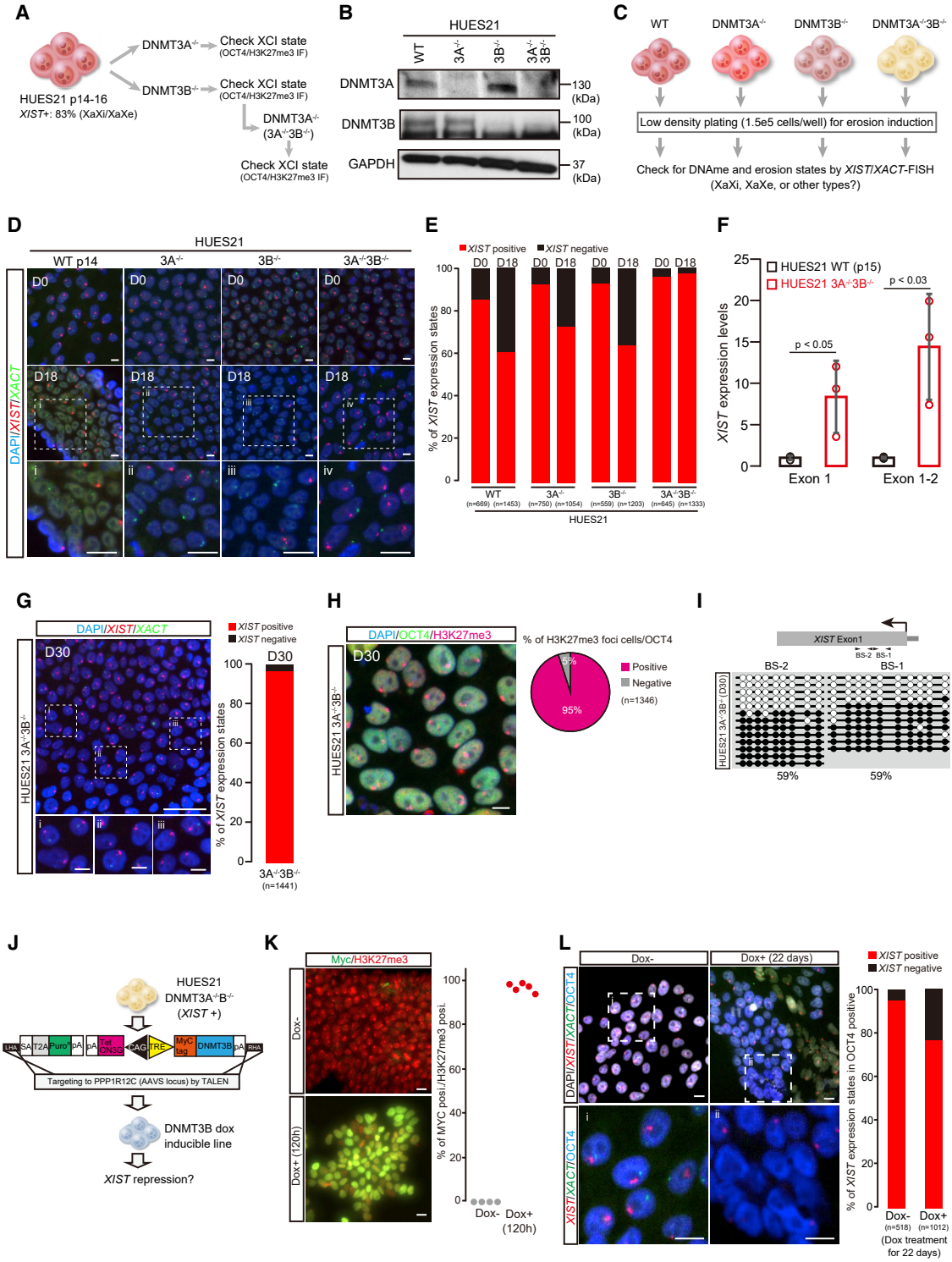

Figure 2. Eliminating DNMT3A/3B prevents erosion of dosage compensation

(A) Experimental scheme for generation of single DNMT3A, single DNMT3B, and double knockout lines. All the knockout lines were produced by the CRISPR-Cas9 system. The *XIST*-positive line HUES21 p14-16 was used as the parental line. After genotyping, OCT4/H3K27me3 immunofluorescence was used to determine XCI state in each clone. See also Figure S2B.

(B) Western blotting for DNMT3A and DNMT3B. GAPDH was used as the loading control. In DNMT3B, the upper band is the targeted size.

(legend continued on next page)

2015), by RNA-FISH (Figures 2C–2E). The quantification of *XIST* and *XACT* transcripts revealed that over the same growth period, a significantly large number of wild-type, single 3A$^{-/-}$, and single 3B$^{-/-}$ mutant cells had lost *XIST* expression and begun to express *XACT* from the eroded X chromosome (Figures 2C–2E). In striking contrast, >95% of *DNMT3A/B* compound mutant cells retained expression of *XIST* on the inactive X chromosome and *XACT* on the one presumptive active X (Figures 2C–2E). Protection of *XIST* expression levels in DNMT3A$^{-/-}$3B$^{-/-}$ compound mutant cells after sustained culture was also readily detected by *XIST* qRT-PCR compared with the wild-type HUES21 clone that had undergone erosion of dosage compensation while being grown in parallel (Figure 2F).

To test the durability of the protection from erosion of dosage compensation conferred by eliminating DNMT3A and DNMT3B, we continued to culture the double-mutant cells for a total of 30 days and found that the inactive X chromosome was still properly maintained in >95% of cells as measured by *XIST* RNA-FISH and immunostaining for H3K27me3 (Figures 2G and 2H). We also determined that a small proportion of cells exhibited no *XIST* expression; however, this was likely the result of experimental detection efficiency, since it was also observed in human primary fibroblasts (Figure 1A). DNA methylation at the *XIST* locus revealed that DNTM3A$^{-/-}$;DNMT3B$^{-/-}$ mutant cells maintained methylation levels appropriately on 50% of sequences analyzed (Figure 2I), similar to the status of DNA methylation in the non-eroded wild type (Figure 1A).

To confirm that the protection from erosion of dosage compensation observed in double *DNMT3A/3B* mutants was due to the loss of methyltransferase activity, we rescued *DNMT3B* expression by a doxycycline (dox)-inducible system targeted to the AAVS locus in double *DNMT3A/3B* mutants of the HUES21 line (Figures 2J–2L). In the absence of dox, these cells retained a clear inactive X as measured by *XIST* expression (Figure 2L). However, upon dox addition and induction of DNMT3B expression, the cells rapidly began to lose *XIST* expression (Figures 2K and 2L).

We further examined whether deletion of *DNMT3A/3B* can prevent erosion of dosage compensation in different female hPSC lines. Using the ADSC-iPS line derived from adipose stem cells with XCI maintained in most early passage cells, while *XACT* biallelic expression was observed at high passage (Figures S2C and S2D), we generated homogeneous DNMT3A$^{-/-}$3B$^{-/-}$ mutant cells using the population with a high proportion of XCI-positive cells (Figures S2C–S2F). Thirty days after low-density plating to induce erosion, we examined XCI state by immunostaining for H3K27me3 and OCT4 (Figure S2G). The DNMT3A$^{-/-}$3B$^{-/-}$ ADSC-iPS line maintained H3K27me3 foci in >95% of OCT4-positive cells, while the wild type exhibited a lower population with H3K27me3 foci (Figure S2H). Taken together, our findings clearly demonstrate that elimination of both *de novo* DNA methyltransferases prevents *XIST* silencing, leading to the erosion of dosage compensation.

Deletion of DNMT3A/3B does not cause global overdosage of X-linked genes, but the effect on transcriptome status depends on genetic background

Since DNA methylation status and erosion of dosage compensation affects transcriptomes (Mekhoubad et al.,

(C) Experimental scheme for erosion induction and assessment of erosion state.
(D) *XIST/XACT* RNA-FISH assay. At day 18 after low-density plating, each line was analyzed. The scale bar indicates 10 μm.
(E) Quantification of *XIST/XACT* expression state by RNA-FISH. n, number of cells analyzed. A detailed classification of the results is shown in Figure S4A.
(F) qPCR analysis of *XIST* expression level in wild-type (WT) HUES21 p15 and DNMT3A$^{-/-}$3B$^{-/-}$ lines. A t test was used for statistical calculation.
(G) *XIST/XACT* expression state by RNA-FISH in DNMT3A$^{-/-}$3B$^{-/-}$ at day 30 after low-density plating. Note that the DNMT3A$^{-/-}$3B$^{-/-}$ line was cultured for several months for gene editing before the low-density plating experiments. The scale bar represents 50 μm. The scale bars for images (i)–(iii) represent 10 μm. n, number of cells analyzed. The categories of expression state are the same as in (D). Two independent experiments were conducted.
(H) H3K27me3/OCT4 immunofluorescence analysis in DNMT3A$^{-/-}$3B$^{-/-}$ at day 30. The scale bar represents 10 μm. The quantification results of H3K27me3 foci in OCT4-positive cells are shown as a pie chart. n, number of analyzed cells. Two independent experiments were conducted.
(I) DNA methylation (DNAme) state at *XIST* promoter regions in DNMT3A$^{-/-}$3B$^{-/-}$ at day 30. BS-1 and BS-2 indicate CpG regions examined by bisulfite sequence.
(J) Experimental scheme of DNMT3B doxycycline (dox)-inducible system in the HUES21 DNMT3A$^{-/-}$3B$^{-/-}$ line from the AAVS locus.
(K) Immunofluorescence analysis of Myc-tag and H3K27me3 at 120 h after dox treatment. Each dot shows the percentage of MYC-positive cells with H3K27me3 signal in observed areas. Two independent experiments were conducted.
(L) Immunofluorescence combined with *XIST/XACT* RNA-FISH analysis in *DNMT3B* inducible line after long-term dox treatment. The dox treatment was conducted for 22 days. OCT4 was used as the undifferentiated hPSC and *XIST* population was determined by only OCT4-positive cells. Two independent experiments were conducted. A detailed classification of the results is shown in Figure S4B. The scale bars represent 10 μm. n, number of cells analyzed.

2012), we examined the impact of double *DNMT3A/3B* mutants on transcriptional profiles in female hPSCs. We performed RNA sequencing on non-eroded wild type (*XIST*$^{+}$ population), eroded wild type (*XIST*$^{-}$ population), and DNMT3A$^{-/-}$3B$^{-/-}$ in the ADSC-iPS and HUES21 lines (Figure 3A). We first ascertained whether X chromosome upregulation occurs by deletion of *de novo* DNA methyltransferases. Based on previous studies (Fukuda et al., 2015; Sangrithi et al., 2017), we employed a computational approach to evaluate the expression ratio between X-linked genes and autosomal genes (X:A) at the chromosome scale using the median expression levels of transcripts per million (TPM), which enables the comparison of expression levels among genes in the same sample. Bootstrap analysis showed that the ratios of the eroded ADSC-iPS and HUES21 cell lines were higher than those of the non-eroded wild-type cell lines (Figure 3B), consistent with previous results (Patel *et al.*, 2017). We found that the ratios of the DNMT3A$^{-/-}$3B$^{-/-}$ cell lines were lower than those of the eroded wild type (Figure 3B), suggesting that, unlike eroded lines, X-linked genes are not overexpressed. However, we did not exclude the possibility that the lower ratios of X:A in the DNMT3A$^{-/-}$3B$^{-/-}$ cell lines resulted from the upregulation of autosomal genes. To test this hypothesis, we checked the global expression status of autosomal and X-linked genes. We did not observe significant upregulation of X-linked genes compared with autosomal genes in the DNMT3A$^{-/-}$3B$^{-/-}$ cell lines (Figure S2I); however, it markedly reduced the expression levels of the mutant line in the HUES21 background (Figure S2I). Thus, these results indicated that, unlike in eroded lines, deletion of DNMT3A/3B did not cause global upregulation of X-linked genes.

Next, we explored whether global gene expression status in the mutant cell lines was similar to that in the non-eroded wild-type cell lines. To address the transcriptional similarity, we conducted hierarchical clustering analysis using trimmed mean of M (TMM) values suitable for direct comparisons between different samples (Robinson and Oshlack, 2010). Interestingly, analysis using X-linked genes indicated clear segregation based on XCI state in ADSC-iPS lines rather than genotype (Figure 3C). In contrast, the expression state of X-linked genes in the HUES21 line was markedly affected by *DNMT3A/3B* mutations (Figure 3C), consistent with a previous study using male hPSCs (Liao et al., 2015). Similarly, hierarchical clustering analysis using all transcripts, including autosomal genes, also separated ADSC-iPS by XCI state and HUES21 by genotype (Figure 3D). We also confirmed the same results when using the TPM normalization method (not shown). Consistent with the clustering results, the mean absolute deviation in the expression ratio of the eroded wild-type cell lines compared with the non-eroded wild-type cell lines was greater than that of DNMT3A$^{-/-}$3B$^{-/-}$ cells in the ADSC-iPS background, while it was greater in DNMT3A$^{-/-}$3B$^{-/-}$ cells in the HUES21 background (Figure 3E).

Taken together, deletion of DNMT3A/3B in non-eroded cell lines does not cause global overdosage of X-linked genes in DNMT3A$^{-/-}$3B$^{-/-}$ cells, but the similarity of global transcriptional status of DNMT3A$^{-/-}$3B$^{-/-}$ cell to non-eroded cell differs in the cell lines.

Loss of DNMT3A and DNMT3B cannot reactivate *XIST* after erosion of dosage compensation

Once established by *de novo* methylation, patterns of DNA methylation are generally maintained by *DNMT1* (Law and Jacobsen, 2010). However, we considered the possibility that eliminating one or both *de novo* DNA methyltransferases after erosion of dosage compensation might still rescue X inactivation (Figure 4A). To address this possibility, we generated wild-type, DNMT3A$^{-/-}$, DNMT3B$^{-/-}$, and DNMT3A$^{-/-}$3B$^{-/-}$ compound mutant sub-clones from a later passage of HUES21 (p34), which had undergone dosage compensation and completely lacked *XIST* expression (Figure 4A). After genotyping and confirming the mutations by western blot analysis (Figures 4B and S2J), we performed prolonged cell culture and then examined the X chromosome (Figure 4C). Unfortunately, we did not find evidence for restoration of dosage compensation by measurement of *XIST*/*XACT* RNA-FISH (Figures 4D and 4E), immunostaining for H3K27me3 (Figure S2K), or *XIST* DNA methylation (Figure 4F). Thus, it appears that once ectopic DNA methylation is established by DNMT3A or DNMT3B and *XIST* expression is silenced, it is faithfully maintained, likely by *DNMT1*, even in the absence of the *de novo* methyltransferases (Figure 4G).

XIST reactivation by the CRISPR activation system cannot reinitiate heterochromatinization

Because ectopic *XIST* expression can reinitiate heterochromatinization *in cis* (Jiang et al., 2013), we considered whether endogenous *XIST* activation by the CRISPR activation (CRISPRa) system would be a useful approach to rescue dosage compensation in eroded female hPSC lines. Using the dCas9:VPR:T2A:GFP fusion gene with the dox-inducible system at the AAVS safe harbor locus (Hazelbaker et al., 2020), we generated *XIST*-inducible lines from the iPS18a line that showed complete *XIST* loss by RNA-FISH (Figures S3A and 1A). We used U6 promoter-driven expression of guide RNAs (gRNAs) that were specific to the *XIST* promoter region from an additional PiggyBac transgene, which also encoded a constitutive red fluorescent reporter gene (Figure S3B). We also assessed whether there was a potential bias in the genomic sequence for gRNA binding, revealing the absence of single-nucleotide variance at the

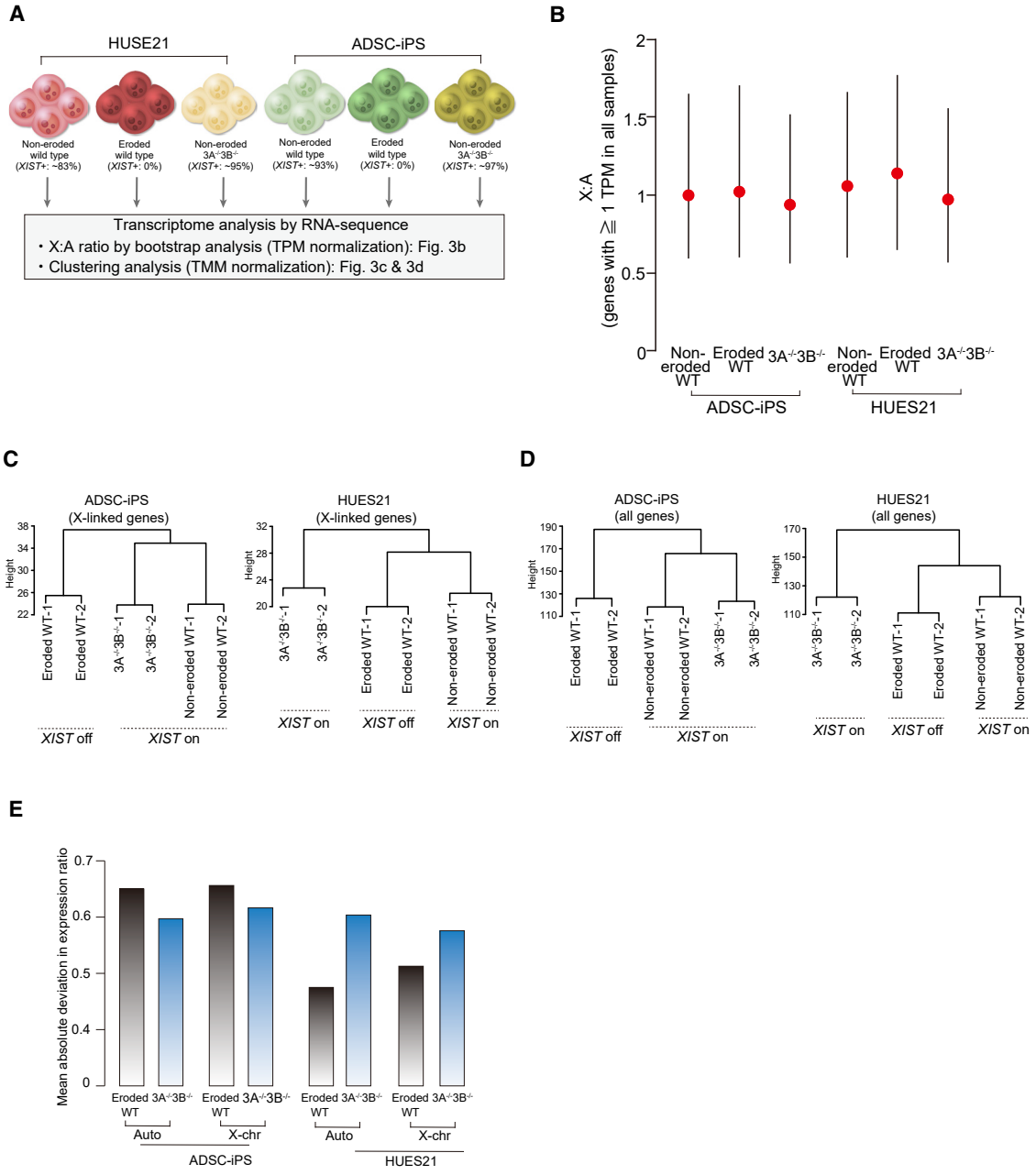

Figure 3. Influence of *DNMT3A* and *DNMT3B* double mutations on transcriptional status

(A) Experimental scheme for RNA-sequence analysis. Non-eroded (wild type), eroded (wild type), and DNMT3A$^{-/-}$3B$^{-/-}$ in the HUES21 and ADSC-iPS lines were used for the assay. In each line, two replicates were analyzed.

(B) Bootstrapped X:A ratios in each cell line. Genes with $\geq$1 TPM in all cell lines were used for the assay. X:A ratios with 95% confidence intervals are shown and the mean ratio is indicated by a red circle.

(C and D) Hierarchical clustering analysis using X-linked genes (C) and all genes (D). TMM normalization was employed and genes with >1 TMM in each cell line were used.

(E) Bar plot illustrating the mean absolute deviation in expression ratios of eroded or DNMT3A$^{-/-}$3B$^{-/-}$ cell lines compared with non-eroded wild-type cell lines. The genes used in the hierarchical clustering analysis were used for the calculation.

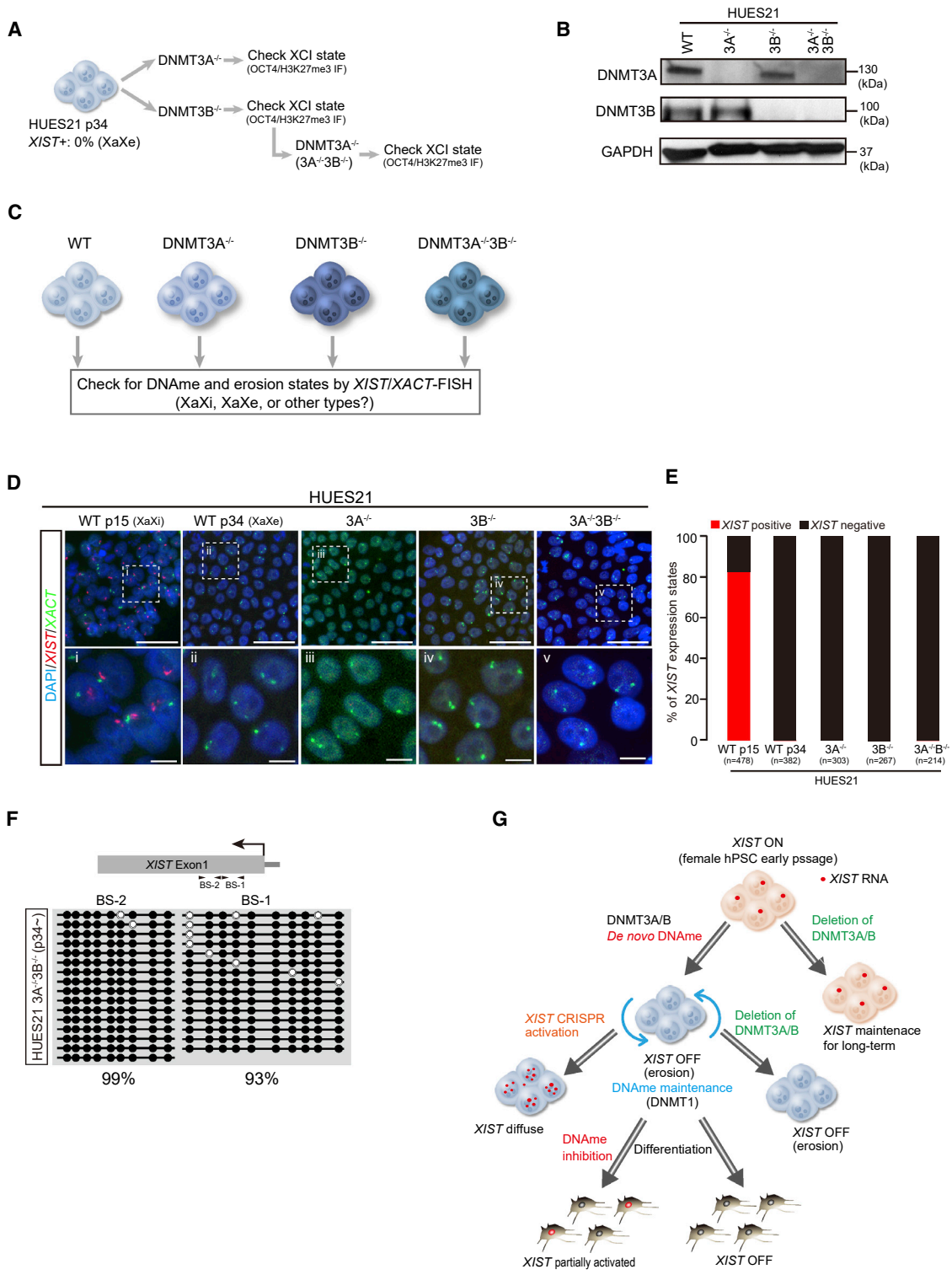

Figure 4. DNMT3A/3B deletion does not rescue *XIST* expression after dosage compensation erosion

(A) Experimental scheme for the generation of DNMT3A/3B knockout lines. HUES21 p34 (*XIST*$^{+}$ 0%) was used as the parental line.

(B) Western blotting for DNMT3A and DNMT3B. GAPDH was used as the loading control.

(C) Experimental scheme to examine the effect of deletion of *de novo* DNA methyltransferases on eroded lines.

(D) *XIST/XACT* RNA-FISH assay. Scale bars represent 10 μm.

(legend continued on next page)

three gRNA sites (Figure S3C). To validate this system, we performed chromatin immunoprecipitation with antibodies specific to the Cas9 protein, followed by quantitative PCR (qPCR). Upon dox induction of Cas9:VPR expression, we found it localized to two *XIST* promoter regions adjacent to the sites of gRNA complementarity, but not to a region farther 5′ of the promoter nor to a region downstream in exon 1 (Figure S3D).

We next examined *XIST* expression by qPCR at 48 and 96 h post-dox induction in two independent clones (iPS18a *XIST*i-1 and iPS18a *XIST*i-2). At 48 h after dox administration, we found an increase in *XIST* expression (>89-fold in iPS18a*XIST*i-1 and >9-fold in iPS18a*XIST*i-2), which continued to increase to significance at 96 h compared with the no-dox control (Figure S3E). These results demonstrated that the dCas9-VPR system could induce endogenous *XIST* expression.

We performed *XIST* RNA-FISH to ask whether the *XIST* transcripts induced by CRISPRa could localize to either the eroded or the active X chromosome and reinitiate heterochromatization. However, upon dox induction of CRISPRa, the *XIST* signal became clearly detected by FISH in 20% of 18a cells from each of the two independent clones (Figures S3F–S3H). We noted that this failure to detect *XIST* in the majority of cells was not due to transgene silencing, as both GFP and RFP were widely expressed after dox administration (Figure S3B). We further noted that, in the CRISPRa cells in which we did observe *XIST* signal, *XIST* did not localize to a clear single focus of expression, as it did in the control cell line with an inactive X (HUES21). Instead, after CRISPRa, *XIST* was expressed in a diffuse pattern throughout the nucleus (Figure S3H). Moreover, at 96 h of dox treatment, immunostaining with antibodies specific for H3K27me3 failed to detect signs of reinitiation of heterochromatin formation on the X (Figure S3I). To rule out the possibility that CRISPRa had simply failed to induce sufficient *XIST* expression to reinactivate the eroded X chromosome, we transfected additional dCas9-VPR and gRNA transgenes into the iPS18a*XIST*i-1 cell line (Figure S3J). After 48 h of dox induction in the cells, qPCR analysis revealed that the *XIST* expression levels were significantly elevated and were >60% of those in HUES21 cells (p13) (Figure S3K). Despite this further increase in expression, RNA-FISH still revealed an unusual localization for *XIST*, with many cells showing strong punctate signals throughout the nucleus, which again failed to colocalize with H3K27me3 (Figures S3L and S3M). Thus, while we had been successful in using CRISPRa to reactivate *XIST* expression in stem cells that had undergone X chromosome erosion, we found it could not reinitiate dosage compensation.

DISCUSSION

Erosion of dosage compensation is one of the single largest sources of epigenetic as well as functional variation in the behavior of female pluripotent stem cells and their differentiated derivatives (Mekhoubad et al., 2012). It would therefore be beneficial for translational stem cell applications if a path could be found for preventing this process from occurring. Given our findings that *DNMT3A/3B* initiate erosion of dosage compensation and the known importance of these enzymes for stem cell differentiation (Ziller et al., 2018), transient or reversible repression of these enzymes during hPSC culture might be useful.

Another interesting observation in our study was the diffuse *XIST* RNA induced by the CRISPR activation system. The aberrant transcribed RNA behavior suggested that *XIST* RNA from a silenced allele(s) might not interact with factors required for *cis* action. Among the proteins that interact with *XIST* RNA, YY1, SAF-A, and CIZ1 are involved in *XIST*/*Xist* RNA diffusion (Loda and Heard, 2019). Since the effect of *XIST* RNA diffusion depends on cell lines (Kolpa et al., 2016), YY1 and CIZ1 are thought to be candidates responsible for the failure of XIST RNA *cis* action by the CRISPR activation system. Given that both YY1 and CIZ1 are highly expressed in female eroded hPSC lines (RNA-sequencing data not shown), protein binding to the *XIST* genomic region might be prevented in the eroded cell line. Although CIZ1 binding to the *Xist* genome depends on repeat E in mice (Loda and Heard, 2019), it remains unknown whether repeat E mutations or epigenetic modifications occur during erosion. In contrast, YY1 binds to *XIST* promoter regions in a DNA-methylation-dependent manner (Makhlouf et al., 2014). Considering our findings that *XIST* expression depends on DNA methylation, unbinding of YY1 to the promoter regions might be one of the causes of the diffusion of *XIST* RNA by the CRISPR activation system.

(E) Quantification of *XIST*/*XACT* expression state. n means the number of cells analyzed. A detailed classification of the results is shown in Figure S4C. Two independent experiments were conducted.

(F) DNA methylation state at *XIST* promoter regions in DNMT3A$^{-/-}$3B$^{-/-}$ generated using eroded HUES21 p34.

(G) Model of *XIST* silencing to initiate erosion in female hPSCs. *De novo* DNA methyltransferases methylate *XIST* to silence its expression. Once *XIST* is silenced, deletion of DNMT3A/3B cannot reactivate *XIST* and the states are stably maintained, likely by DNMT1. During differentiation, demethylation can partially reactivate *XIST*, but forced activation of endogenous *XIST* in eroded hPSCs generates diffused transcripts that cannot act to cause heterochromatization.

Given that erosion of dosage compensation occurs in female hPSC lines, it might be tempting to prioritize the use of male cells for the development of allogenic or other therapies. However, we argue that if women are to optimally and equally benefit from future hPSC therapies, especially autologous therapies, it must remain a priority to develop methods to eliminate erosion of dosage compensation.

EXPERIMENTAL PROCEDURES

hPSC culture

HUES21 and iPS18a lines were cultured in mTeSer medium (STEMCELL Technologies) without feeder cells or on irradiated CF1 mouse embryonic fibroblasts (Thermo Fisher Scientific) with standard hPSC medium. The detailed description is provided in the supplemental experimental procedures.

Motor neuron differentiation

Motor neuron differentiation was performed based on a previous report (Klim et al., 2019). The detailed description is provided in the supplemental experimental procedures.

Generation of single DNMT3A, single DNMT3B, and double knockout lines

For the generation of DNMT3A/3B knockout lines, we used the CRISPR-Cas9 system with the gRNAs previously validated (Liao et al., 2015). The detailed description is provided in the supplemental experimental procedures.

RNA-FISH

RNA-FISH experiments were performed based on a previous report (Fukuda et al., 2016). The detailed description of the method and classification of the results are provided in the supplemental experimental procedures and Figures S4A–S4C, respectively.

Data and code availability

RNA-sequencing data from this study have been deposited in the GEO database (GSE160454).

SUPPLEMENTAL INFORMATION

Supplemental information can be found online at https://doi.org/10.1016/j.stemcr.2021.07.015.

AUTHOR CONTRIBUTIONS

A.F. and K.E. conceived and designed the study. A.F. generated all of gene-manipulated cell lines, developed the construct for the 18a*XIST*i lines, and conducted most of the experiments and analysis. D.H., A.B., P.M., A.M., and L.B. designed and developed constructs and tools for generation of CRISPRa 18a*XIST*i lines and analyzed the data. N.M. and C.O. analyzed data and helped in the generation of gene-manipulated cell lines, FISH, and western blotting experiments. H.A. and A.U. generated the ADSC-iPS line. J.H. helped culture cells and in western blotting experiments. F.L. helped culture cells. I.G. helped with differentiation experiments. M.Q. helped with western blotting and immunofluorescence staining experiments. A.F. and K.E. wrote the manuscript with input from all coauthors.

CONFLICT OF INTERESTS

K.E. is a cofounder of Q-State Biosciences, Quralis, and Enclear Therapies, and is group vice president at BioMarin Pharmaceutical.

ACKNOWLEDGMENTS

We would like to thank G. Pintacuda, J. Klim, and H. Kobayashi for their helpful discussion and S. Kikugawa for assistance in bioinformatic analysis. We also thank M. Charlton for her assistance in many aspects of this study. A.F. was supported by JSPS Postdoctoral Fellowships for Research Abroad and is currently supported by the JSPS Leading Initiative for Excellent Young Researchers (LEADER) and by AMED under grant JP21bm0704038. K.E. was supported by grants from the NIGMS P01 (grant GM099117) and the Stanley Center for Psychiatric Research at the Broad Institute.

Received: May 11, 2021
Revised: July 21, 2021
Accepted: July 21, 2021
Published: August 19, 2021

REFERENCES

Anguera, M.C., Sadreyev, R., Zhang, Z., Szanto, A., Payer, B., Sheridan, S.D., Kwok, S., Haggarty, S.J., Sur, M., Alvarez, J., et al. (2012). Molecular signatures of human induced pluripotent stem cells highlight sex differences and cancer genes. Cell Stem Cell *11*, 75–90. https://doi.org/10.1016/j.stem.2012.03.008.

Augui, S., Nora, E.P., and Heard, E. (2011). Regulation of X-chromosome inactivation by the X-inactivation centre. Nat. Rev. Genet. *12*, 429–442. https://doi.org/10.1038/nrg2987.

Chapman, A.G., Cotton, A.M., Kelsey, A.D., and Brown, C.J. (2014). Differentially methylated CpG island within human XIST mediates alternative P2 transcription and YY1 binding. BMC Genet. *15*, 89. https://doi.org/10.1186/s12863-014-0089-4.

Christman, J.K. (2002). 5-Azacytidine and 5-aza-2′-deoxycytidine as inhibitors of DNA methylation: mechanistic studies and their implications for cancer therapy. Oncogene *21*, 5483–5495. https://doi.org/10.1038/sj.onc.1205699.

Csankovszki, G., Nagy, A., and Jaenisch, R. (2001). Synergism of Xist RNA, DNA methylation, and histone hypoacetylation in maintaining X chromosome inactivation. J. Cell Biol. *153*, 773–784. https://doi.org/10.1083/jcb.153.4.773.

Fukuda, A., Mitani, A., Miyashita, T., Sado, T., Umezawa, A., and Akutsu, H. (2016). Maintenance of xist imprinting depends on chromatin condensation state and Rnf12 dosage in mice. PLoS Genet. *12*, e1006375. https://doi.org/10.1371/journal.pgen.1006375.

Fukuda, A., Tanino, M., Matoba, R., Umezawa, A., and Akutsu, H. (2015). Imbalance between the expression dosages of X-chromosome and autosomal genes in mammalian oocytes. Sci. Rep. *5*, 14101. https://doi.org/10.1038/srep14101.

Guo, G., von Meyenn, F., Rostovskaya, M., Clarke, J., Dietmann, S., Baker, D., Sahakyan, A., Myers, S., Bertone, P., Reik, W., et al. (2017). Epigenetic resetting of human pluripotency. Development *144*, 2748–2763. https://doi.org/10.1242/dev.146811.

Hazelbaker, D.Z., Beccard, A., Angelini, G., Mazzucato, P., Messana, A., Lam, D., Eggan, K., and Barrett, L.E. (2020). A multiplexed gRNA piggyBac transposon system facilitates efficient induction of CRISPRi and CRISPRa in human pluripotent stem cells. Sci. Rep. *10*, 635. https://doi.org/10.1038/s41598-020-57500-1.

Jiang, J., Jing, Y., Cost, G.J., Chiang, J.C., Kolpa, H.J., Cotton, A.M., Carone, D.M., Carone, B.R., Shivak, D.A., Guschin, D.Y., et al. (2013). Translating dosage compensation to trisomy 21. Nature *500*, 296–300. https://doi.org/10.1038/nature12394.

Klim, J.R., Williams, L.A., Limone, F., Guerra San Juan, I., Davis-Dusenbery, B.N., Mordes, D.A., Burberry, A., Steinbaugh, M.J., Gamage, K.K., Kirchner, R., et al. (2019). ALS-implicated protein TDP-43 sustains levels of STMN2, a mediator of motor neuron growth and repair. Nat. Neurosci. *22*, 167–179. https://doi.org/10.1038/s41593-018-0300-4.

Kolpa, H.J., Fackelmayer, F.O., and Lawrence, J.B. (2016). SAF-A requirement in anchoring XIST RNA to chromatin varies in transformed and primary cells. Dev. Cell *39*, 9–10. https://doi.org/10.1016/j.devcel.2016.09.021.

Law, J.A., and Jacobsen, S.E. (2010). Establishing, maintaining and modifying DNA methylation patterns in plants and animals. Nat. Rev. Genet. *11*, 204–220. https://doi.org/10.1038/nrg2719.

Liao, J., Karnik, R., Gu, H., Ziller, M.J., Clement, K., Tsankov, A.M., Akopian, V., Gifford, C.A., Donaghey, J., Galonska, C., et al. (2015). Targeted disruption of DNMT1, DNMT3A and DNMT3B in human embryonic stem cells. Nat. Genet. *47*, 469–478. https://doi.org/10.1038/ng.3258.

Liu, X., Nefzger, C.M., Rossello, F.J., Chen, J., Knaupp, A.S., Firas, J., Ford, E., Pflueger, J., Paynter, J.M., Chy, H.S., et al. (2017). Comprehensive characterization of distinct states of human naive pluripotency generated by reprogramming. Nat. Methods *14*, 1055–1062. https://doi.org/10.1038/nmeth.4436.

Loda, A., and Heard, E. (2019). Xist RNA in action: past, present, and future. PLoS Genet. *15*, e1008333. https://doi.org/10.1371/journal.pgen.1008333.

Makhlouf, M., Ouimette, J.F., Oldfield, A., Navarro, P., Neuillet, D., and Rougeulle, C. (2014). A prominent and conserved role for YY1 in Xist transcriptional activation. Nat. Commun. *5*, 4878. https://doi.org/10.1038/ncomms5878.

Marahrens, Y., Panning, B., Dausman, J., Strauss, W., and Jaenisch, R. (1997). Xist-deficient mice are defective in dosage compensation but not spermatogenesis. Genes Dev. *11*, 156–166.

Meissner, A. (2010). Epigenetic modifications in pluripotent and differentiated cells. Nat. Biotechnol. *28*, 1079–1088. https://doi.org/10.1038/nbt.1684.

Mekhoubad, S., Bock, C., de Boer, A.S., Kiskinis, E., Meissner, A., and Eggan, K. (2012). Erosion of dosage compensation impacts human iPSC disease modeling. Cell Stem Cell *10*, 595–609. https://doi.org/10.1016/j.stem.2012.02.014.

Patel, S., Bonora, G., Sahakyan, A., Kim, R., Chronis, C., Langerman, J., Fitz-Gibbon, S., Rubbi, L., Skelton, R.J.P., Ardehali, R., et al. (2017). Human embryonic stem cells do not change their X inactivation status during differentiation. Cell Rep. *18*, 54–67. https://doi.org/10.1016/j.celrep.2016.11.054.

Robinson, M.D., and Oshlack, A. (2010). A scaling normalization method for differential expression analysis of RNA-seq data. Genome Biol. *11*, R25. https://doi.org/10.1186/gb-2010-11-3-r25.

Sahakyan, A., Kim, R., Chronis, C., Sabri, S., Bonora, G., Theunissen, T.W., Kuoy, E., Langerman, J., Clark, A.T., Jaenisch, R., and Plath, K. (2017). Human naive pluripotent stem cells Model X chromosome dampening and X inactivation. Cell Stem Cell *20*, 87–101. https://doi.org/10.1016/j.stem.2016.10.006.

Sahakyan, A., Yang, Y., and Plath, K. (2018). The role of xist in X-chromosome dosage compensation. Trends Cell Biol. *28*, 999–1013. https://doi.org/10.1016/j.tcb.2018.05.005.

Salomonis, N., Dexheimer, P.J., Omberg, L., Schroll, R., Bush, S., Huo, J., Schriml, L., Ho Sui, S., Keddache, M., Mayhew, C., et al. (2016). Integrated genomic analysis of diverse induced pluripotent stem cells from the progenitor cell biology consortium. Stem Cell Rep. *7*, 110–125. https://doi.org/10.1016/j.stemcr.2016.05.006.

Sangrithi, M.N., Royo, H., Mahadevaiah, S.K., Ojarikre, O., Bhaw, L., Sesay, A., Peters, A.H., Stadler, M., and Turner, J.M. (2017). Non-canonical and sexually dimorphic X dosage compensation states in the mouse and human germline. Dev. Cell *40*, 289–301 e283. https://doi.org/10.1016/j.devcel.2016.12.023.

Smith, Z.D., Chan, M.M., Humm, K.C., Karnik, R., Mekhoubad, S., Regev, A., Eggan, K., and Meissner, A. (2014). DNA methylation dynamics of the human preimplantation embryo. Nature *511*, 611–615. https://doi.org/10.1038/nature13581.

Szyf, M. (2011). The implications of DNA methylation for toxicology: toward toxicomethylomics, the toxicology of DNA methylation. Toxicol. Sci. *120*, 235–255. https://doi.org/10.1093/toxsci/kfr024.

Vallot, C., Ouimette, J.F., Makhlouf, M., Feraud, O., Pontis, J., Come, J., Martinat, C., Bennaceur-Griscelli, A., Lalande, M., and Rougeulle, C. (2015). Erosion of X Chromosome inactivation in human pluripotent cells initiates with XACT coating and depends on a specific heterochromatin landscape. Cell Stem Cell *16*, 533–546. https://doi.org/10.1016/j.stem.2015.03.016.

Ziller, M.J., Ortega, J.A., Quinlan, K.A., Santos, D.P., Gu, H., Martin, E.J., Galonska, C., Pop, R., Maidl, S., Di Pardo, A., et al. (2018). Dissecting the functional consequences of de novo DNA methylation dynamics in human motor neuron differentiation and physiology. Cell Stem Cell *22*, 559–574 e559. https://doi.org/10.1016/j.stem.2018.02.012.

Stem Cell Reports, Volume *16*

Supplemental Information

De novo DNA methyltransferases DNMT3A and DNMT3B are essential for *XIST* silencing for erosion of dosage compensation in pluripotent stem cells

Atsushi Fukuda, Dane Z. Hazelbaker, Nami Motosugi, Jin Hao, Francesco Limone, Amanda Beccard, Patrizia Mazzucato, Angelica Messana, Chisa Okada, Irune Guerra San Juan, Menglu Qian, Akihiro Umezawa, Hidenori Akutsu, Lindy E. Barrett, and Kevin Eggan

Supplementary Fig. 1

a

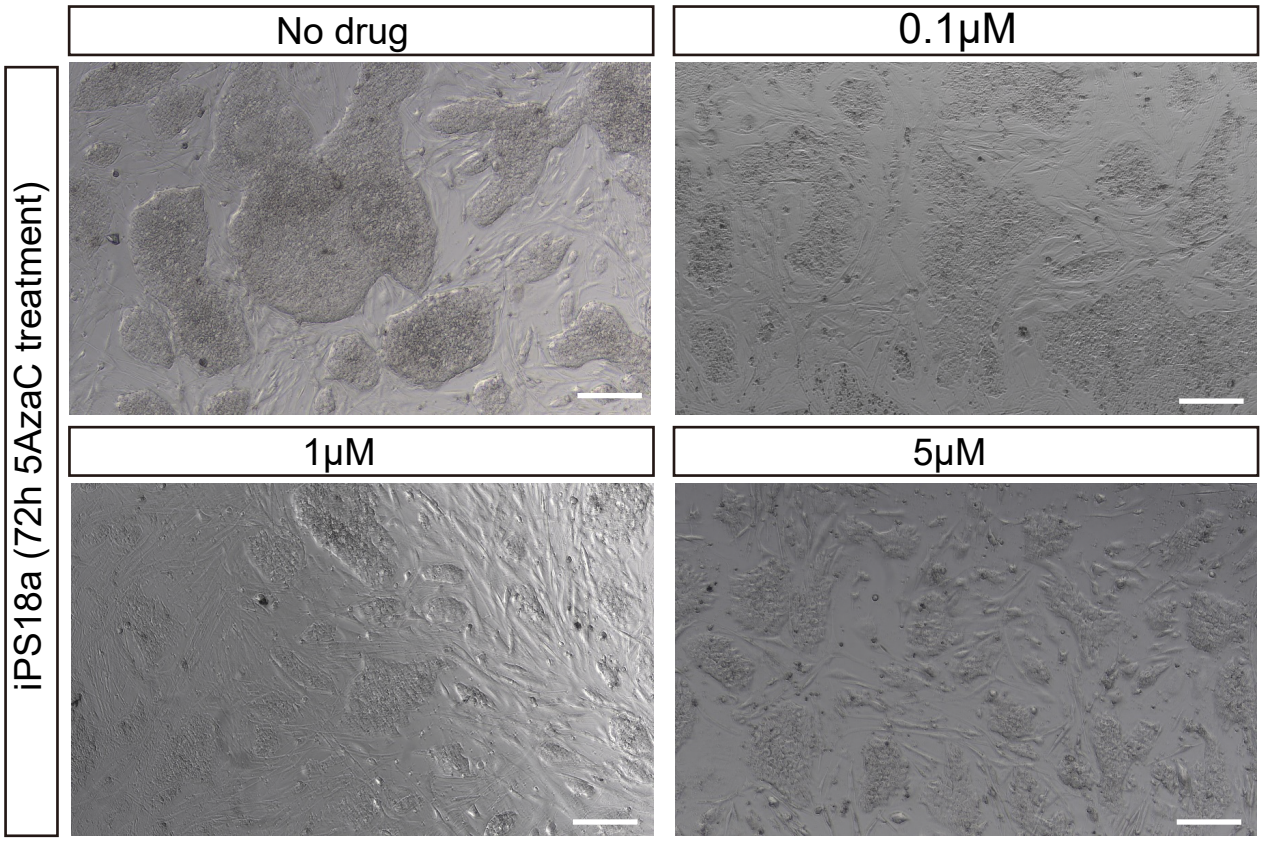

b

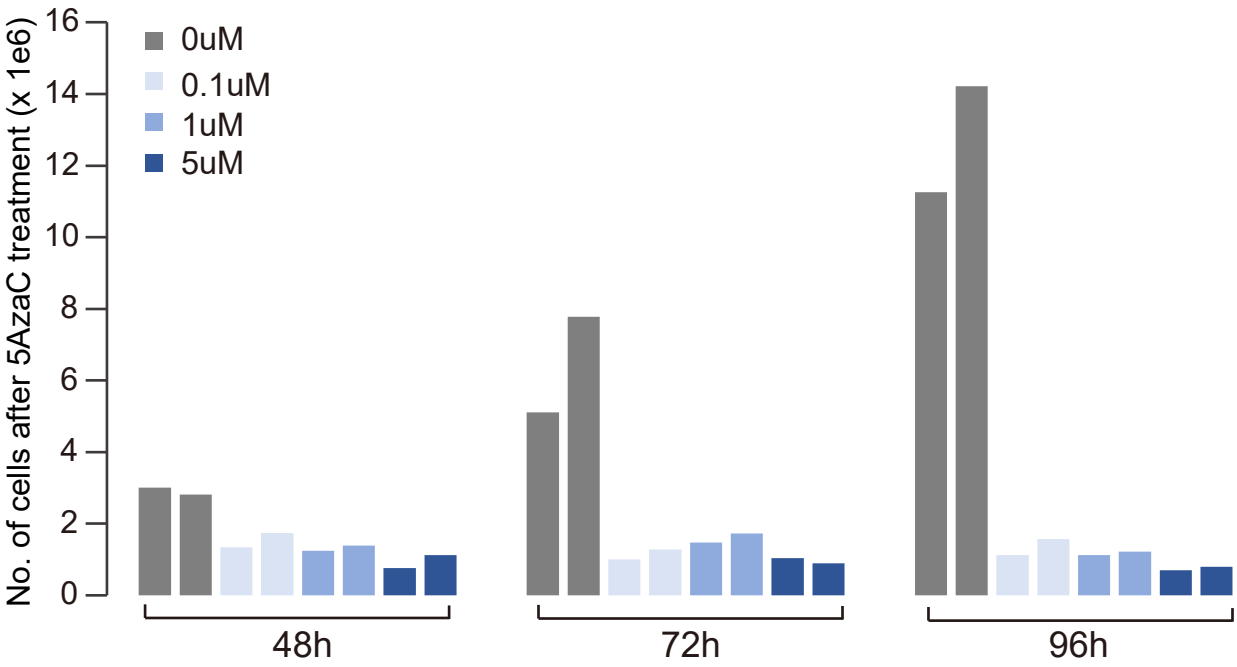

Figure S1. Effect of 5az treatment on hPSCs culture. (a) cultures 72 hours after 5azaC treatment with various concentrations. The scale bar indicates 250 μm. (b) Cell number analysis in each concentration.

Supplementary Fig. 2

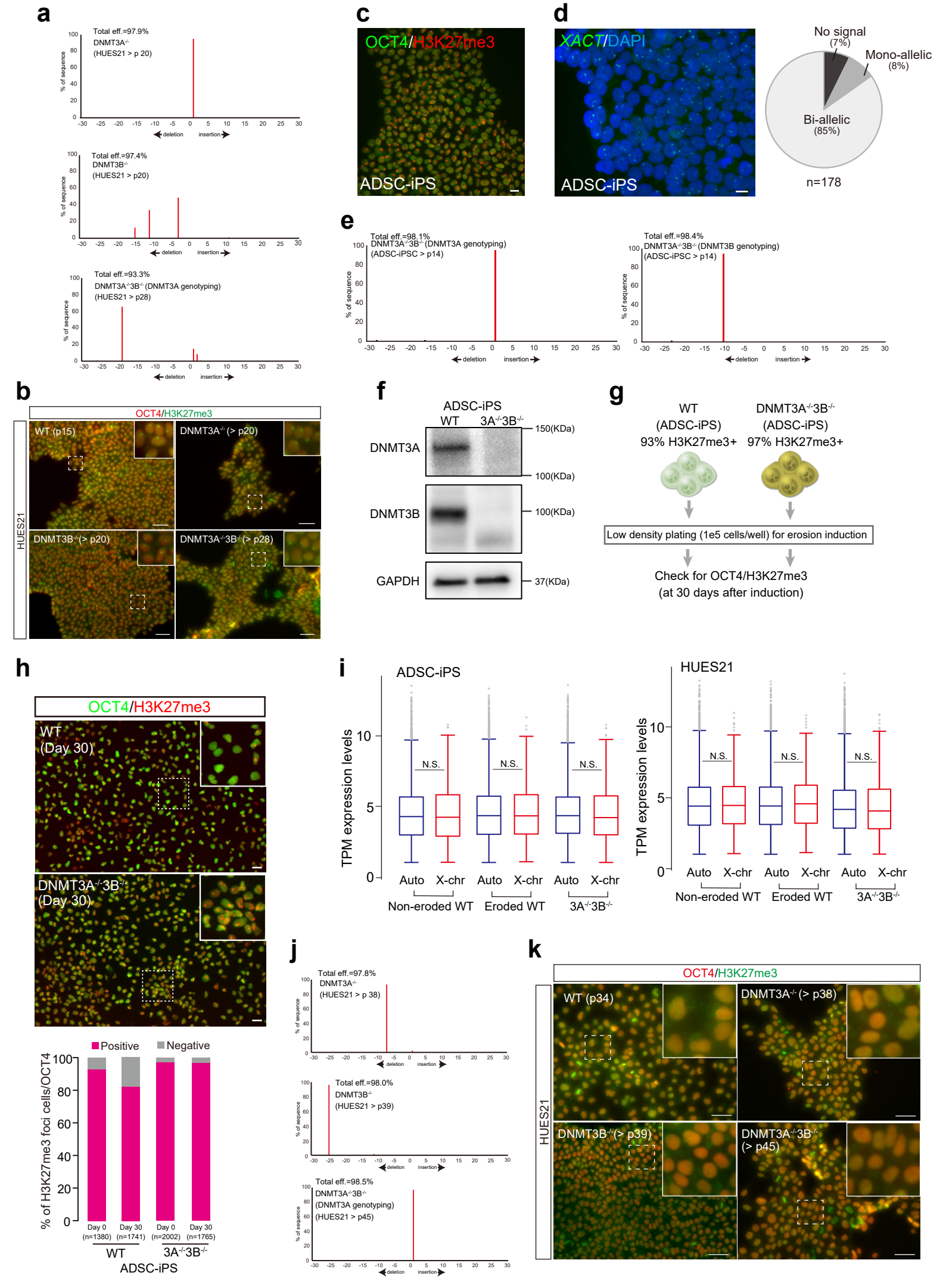

Figure S2. Generation of DNMT3A, 3B, and double knockout liens and RNA-sequencing analysis. (a) Genotyping results by TIDE analysis in HUES21 p14-16 line. (b) Immunofluorescence against OCT4/H3K27me3 in each knockout line derived from HUES21 p14-16. The scale bar indicates 50 μm. (c) H3K27me3/OCT4 staining in ADSC-iPS at p14. The scale bar indicates 20 μm. (d) *XACT* RNA-FISH in ADSC-iPS at p41. n = the number of cells analyzed. The scale bar indicates 10 μm. (e) Genotyping results by TIDE analysis in mutant lines derived from ADSC-iPS at p14. (f) Western blotting for DNMT3A and DNMT3B. GAPDH was used as loading control in mutant lines derived from ADSC-iPS at p14. (g) Experimental scheme for induction of erosion in ADSC-iPS lines. (h) H3K27me3/OCT4 staining 30 days after low-density plating in ADSC-iPS lines. The scale bar indicates 20 μm. Quantification of H3K27me3 foci cells was shown as bar graph. n = the number of cells analyzed. (i) Global gene expression status in each cell line by RNA-sequencing. Boxplots show TPM expression status in autosomal and X-linked genes. The genes used for the bootstrap analysis were measured in ADSC-iPS (left) and HUES21 (right) cell lines. The Wilcoxon rank sum test was used for statistical analysis. N.S. means no significances. (j) Genotyping results by TIDE analysis in DNMT3A, 3B, and double knockout liens derived from HUES21 p34. (k) Immunofluorescence against OCT4/H3K27me3 in each knockout line derived from HUES21 p34. The scale bar indicates 50 μm.

Supplementary Fig. 3

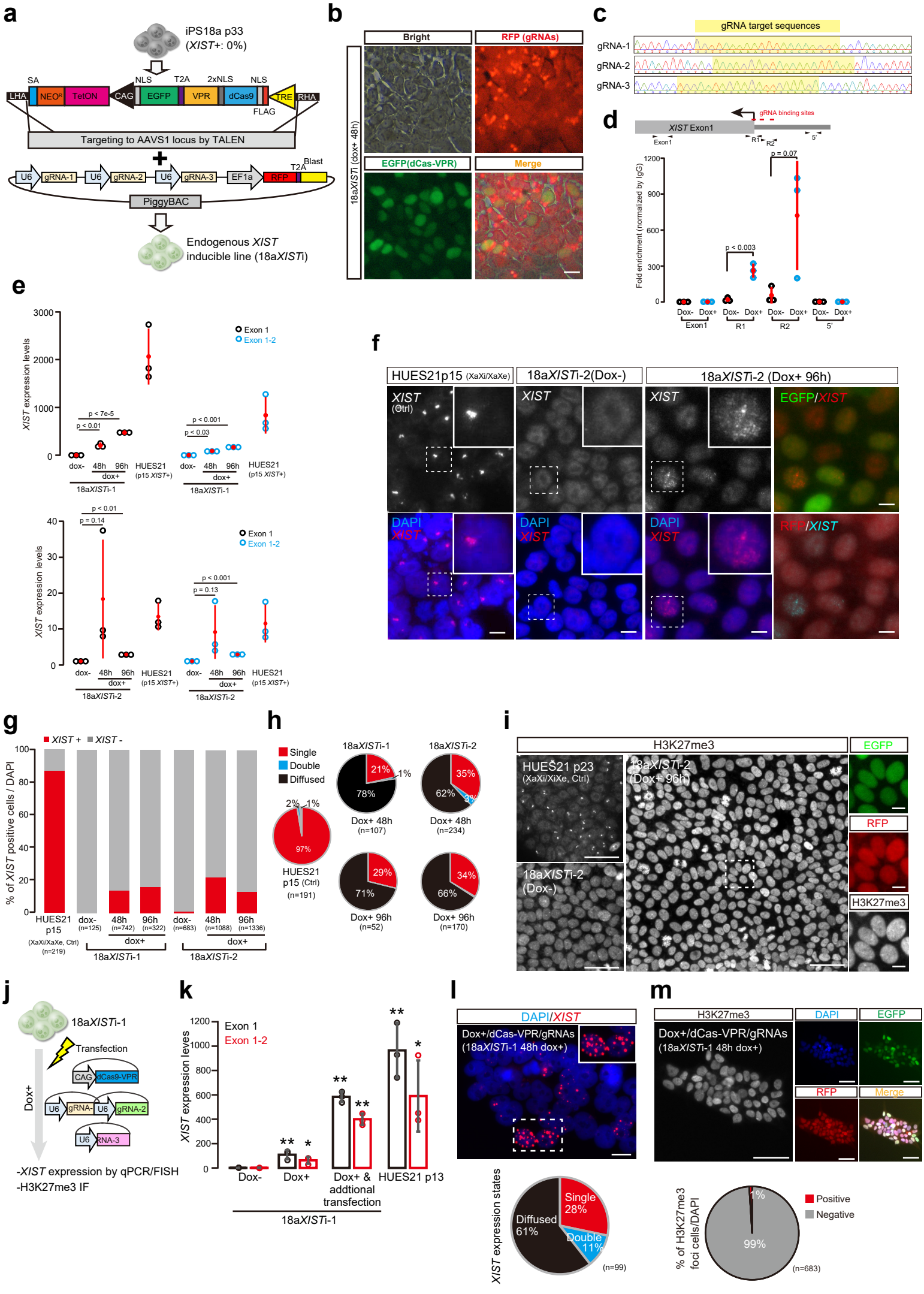

Figure S3. After erosion of dosage compensation CRSPRa can induce *XIST* expression but not restore XCI. (a) Generation of XIST inducible line (18aXISTi) for CRISPR activation studies. (b) Representative images of hPSCs with CRSPRa system after 48 hours of dox administration. The scale bar indicates 10 μm. See also Extended Data Figure 2b and 2c. (c) Sanger sequencing analysis for gRNA target sites. (d) ChIP-qPCR assay using Cas9 antibody. Three red lines indicate gRNA binding sites. The % of input data was normalized using an IgG only control. T-test was conducted for statistical analysis. Red bar indicates average ± SD. T-test was used for statistical calculation. (e) qPCR assay for XIST expression states in inducible lines and HUES21 with XIST positive. The left and right graphs show XIST expression levels of 18aXISTi-1 and 18aXISTi-2 lines, respectively. XIST expression levels were normalized to GAPDH levels. Red bar is average ± SD. T-test was used for statistical calculation. (f) XIST RNA-FISH images. HUES21 p15 (XaXi/XaXe) was used as positive control (Ctrl). The scale bar indicates 10 μm. (g) Quantification of XIST positive cells by RNA-FISH. n=number of cells analyzed. Xa: active X-chr, Xi: inactive X-chr, and Xe: eroded X-chr. (h) Quantification of XIST expression states based on the signals. Diffused state is shown as in (Figure 3e). n = number of cells analyzed. (i) H3K27me3 states in 18aXISTi lines. H3K27me3 immunofluorescence analysis at 96 hours after dox+. HUES21 p23 (XaXi/XaXe) was used as Ctrl. The scale bar indicates 50 μm. The scale bar of enlarged image of is 10 μm. (j) Experimental scheme. Additional dCas9-VPR and three gRNAs are transfected in 18aXISTi-1 line. The cells were cultured with or without dox. At 48 hours after transfection, the cells were analyzed by qPCR, XIST RNA-FISH and H3K27me3 staining. (k) XIST expression states by qPCR analysis. The expression level of dox – sample was set as 1. * and ** indicate $p < 0.05$ and $p < 0.01$, respectively. T-test was used for the statistical calculation. GAPDH was used as internal control for normalization. (l) XIST RNA-FISH in transfected cells with dox treatment for 48 hours. The expression states were based on the signal numbers in the nucleus. n = number of cells analyzed. Scale bar = 10 um. (m) Quantification of H3K27me3 foci in transfected cells with dox treatment for 48 hours. The representative picture is shown. n = number of cells analyzed. The scale bar indicates 50 μm.

Supplementary Fig. 4

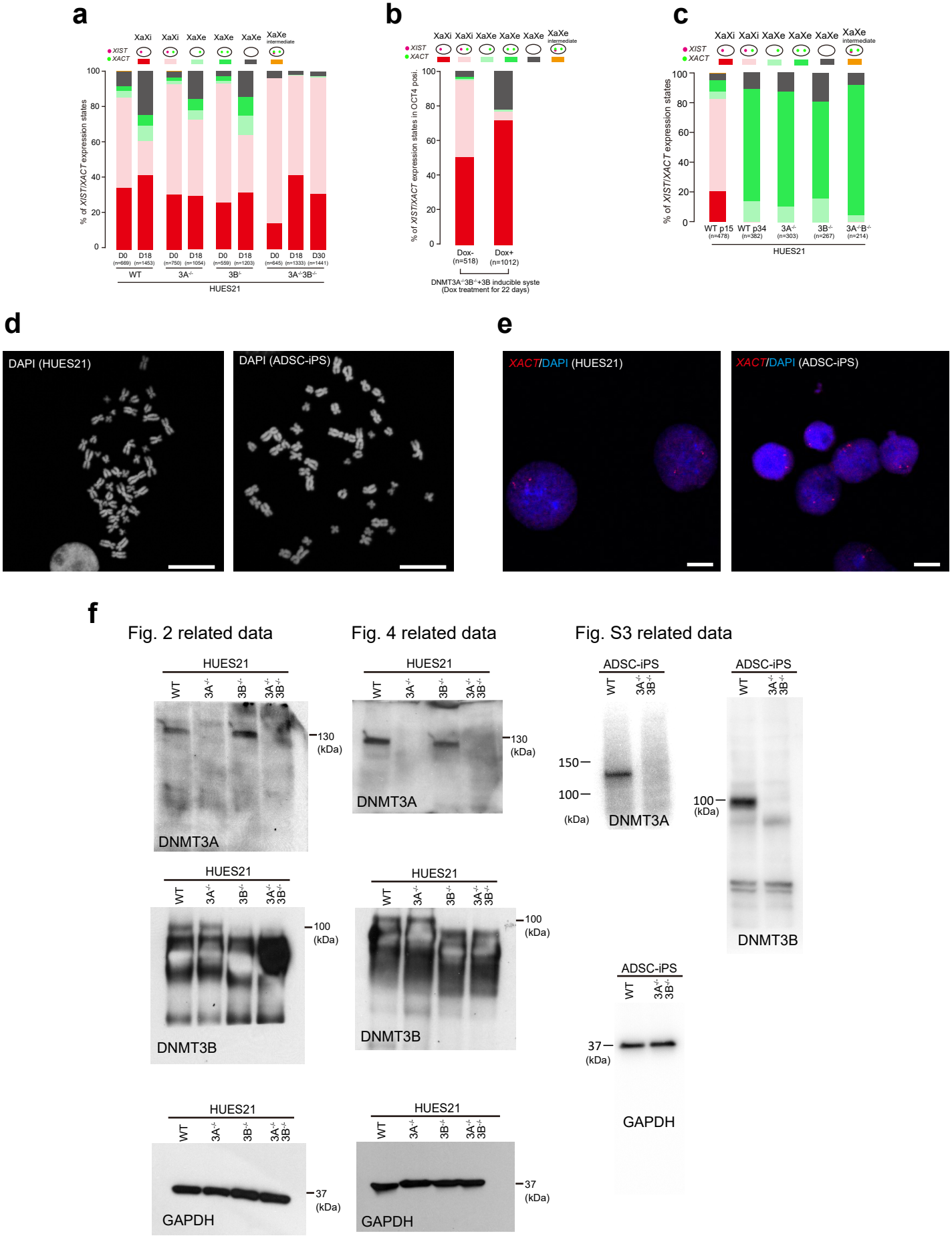

Figure S4. Detailed classification of RNA-FISH results (a-c), chromosome spreading/DNA-FISH (d and e), and uncropped images for western blotting (f). In chromosomal assays, HUES21 (p44) and ADSC-iPS (p56) were used for metaphase spreading (d) and HUES21 (p39) and ADSC-iPS (p52) were used for XACT DNA-FISH experiments, respectively. The scale bar indicates 10 μm. At least 50 cells were analyzed in both assays.

Supplementary Table S1.
Primer sequences

Name	Sequences	Assay
3A_Geno_F1 3A_Geno_R1	CTGTCCCCTCCACCTTCTC TAACCCTGCTTCCTCCCTTTCTA	Genotyping for DNMT3A KO
GF_2 GR_1	GGTAGTGTGACTCGCTCAAGCT GAAGCCCAACACCAGGAAGT	Genotyping for DNMT3B KO
R1_1-F R1_1-R	TTTAATAYGAAAAGTATATAGTAAAGATAAAGAGG TAACRAACTATACTTTATTAAATTATCCAAAATAAC	BS for BS-1 regions
R1_2-F R1_2-R	GTTGTGATTAATTTTATTTTTATTTTTAATTGGTTGGG CATAACRAACCTCTTTATCTTTACTATATAC	BS for BS-2 regions
XIST_E1-2-F XIST_E1-2-R	AGCTCCTCGGACAGCTGTAA GGACACATGCAGCGTGGTA	qPCR for *XIST* mature transcripts
XIST_E1-F XIST_E1-R	TAGCCAGTCAGGAGAAAGAAGTG GACAAATAAGAGGGGACAGAGGT	qPCR for *XIST* immature transcripts
GAPDH-F GAPDH-R	TTGTCAAGCTCATTTCCTGGTATG TCCTCTTGTGCTCTTGCTGG	qPCR for GAPDH
ChIP_e1-F ChIP_e1-R	GATGTAAGCAACGAGGAAGCA GTATTTGTGGACCTGTGTAGGAGAA	ChIP-qPCR for Exon1 regions
ChIP_gRNA-F ChIP_gRNA-R	AGGGCGGAGAGAGCATAAGAG ATAGATGAGAACTGGAAAACCCATT	ChIP-qPCR for R2 regions
ChIP_gRNA-P1-F ChIP_gRNA-P1-R	CAGCCCCGAGAGAGTAAGAAATA ACCAACCAAATCACAAAGATGTC	ChIP-qPCR for R1 regions
5'_XIST-F 5'_XIST-R	AGCAAGAGAGAAAAAGGAAAGAAAG TGGAGGAAATAGGAAAATAGTAAAGA	ChIP-qPCR for Exon4 regions

Experimental procedures

hPSC culture: HUES21 and iPS18a lines were cultured in mTeSer medium (Stem Cell Technology) without feeder cells or on irradiated CF1 mouse embryonic Fibroblasts (Thermofisher Scientific) with standard hPSCs medium containing KO-DMEM (Thermofisher Scientific) supplemented with 20% knockout serum replacement (Thermofisher Scientific), 1% nonesesential amino acids (Thermofisher Scientific), 2 mM glutamax-I (Thermofisher Scientific), 50 units/ml penicillin and 50 ug/ml streptomycin (Thermofisher Scientific), 0.055 mM 2-mercaptoethanol (Thermofisher Scientific), and 20 ng/ml bFGF (Millipore) (Mekhoubad et al., 2012). To establish female ADSC-iPS derived from adipose-derived stromal cells (ADSCs, Lonza Poietics, #PT-5006), mRNA Reprogramming kit (Reprocell, #00-0076) was used according to the manufacturer's instructions. ADSC-iPS line was cultured in StemFlex (Thermofisher Scientific). All cells were culture in 5% CO_2 at 37^{o}C. In the culture with mTeSer medium, Marigel (Corning) and gelatin were used as matrix for mTeSer and standard hPSCs, respectively. For hPSCs passage, 1 mM EDTA (Thermofisher Scientific) was used and 10 μM Y-27632 (Stemgent) was added for 24 hours. Chromosomal normality in high passaged lines was checked by chromosomal spreading and DNA-FISH (Figure S4d and S4e). The hESCs and iPSCs used in this study were previously approved by the institutional review boards of Harvard University, Massachusetts General Hospital, Columbia University, National Center for Child Health and Development, and Tokai University. Our lab regularly checks for mycoplasma contamination using the MycoAlert kit (Lonza) with no cell lines used in this study testing positive. The use of these cells at Harvard was further approved and determined not to constitute Human Subjects Research by the Committee on the Use of Human Subjects in Research at Harvard University.

Motor neuron differentiation: We performed motor neuron differentiation as previously reported

(Klim et al., 2019). In brief, differentiation began once cultured hPSCs became confluent (day 0). The medium was switched to motor neuron differentiation medium (½ Neurobasal (Life Technologies) ½ DMEM-F12 (Life Technologies) supplemented with ×1 B-27 supplement (Gibco), ×1 N-2 supplement (Gibco), ×1 Gibco GlutaMAX (Life Technologies) and 100 µM non-essential amino-acids: NEAA). Treatment with small molecules was conducted as follows: 10 µM SB431542 (Custom Synthesis), 100 nM LDN-193189 (Custom Synthesis), 1 µM retinoic acid (Sigma) and 1 µM Smoothend agonist (Custom Synthesis) on d0–d5; 5 µM DAPT (Custom Synthesis), 4 µM SU-5402 (Custom Synthesis), 1 µM retinoic acid (Sigma) and 1 µM Smoothend agonist (Custom Synthesis) on d6–d14. For the 5azacytidine (Sigma) experiment, 5 µM 5azacytidine was added to differentiation medium from day 3 to day 14.

Generation of *XIST* inducible cell lines (iPS18a*XIST*i) for CRISPR activation system. To create inducible iPS18a*XIST*i lines, 2.5 million iPS18a cells (Harvard University) were transfected with 10 µg TRE3G-dCas9-T2A-EGFP AAVS1 donor plasmid pT076 (Barrett Lab, Broad Institute) along with 1.5 µg AAVS1 TALEN L (Addgene #59025) and 1.5 µg AAVS1 TALEN R (Addgene #59026) via the Neon Electroporation System (ThermoFisher) at 1600 mV, 20 ms, 1 pulses. For the first round of clonal selection, we plated transfected cells at low-density (16,000 cells in a 10 cm dish) under selection with 50 ng/ul G418 (Gibco 10131035) to allow for single-cell colony formation. 10 µM Y-27632 was added to the culture for 14 days. Importantly, cells are kept under selection with 50 ng/ul G418 for the duration of experiments to protect against shutdown of the AAVS1 integrated cassette. In this strategy, colonies are picked and deposited into a 96-well plate and when sufficiently dense, the 96-well plate is triplicated to create 3 plates of identical clones. Plate 1 is frozen for storage, plate 2 is treated with doxycycline (Sigma, D9891-25g) at a final concentration of 2 µg/ml at 24 hours after duplication for visualization of EGFP+ colonies (with high levels of EGFP expression serving as a

proxy for high dCas9 expression), and plate 3 is maintained for expansion and banking of EGFP+ colonies (n=6) while the analysis of plate 2 is performed. Selected clones were genotyped by junction PCR to confirm the on target 5' and 3' integration of the dCas9-VPR cassettes into the AAVS1 locus. Primer sequences for AAVS1 integration are as follows: 5' junction primers GE381 (ACACTCTTTCCCTACACGACGCTCTTCCGATCTAGTCTTCTTCCTCCAACCCG) and GE332 TTCATCCTGCAGCTCGTTCA, 3' junction primers GE223 TCGACTTCCCCTCTTCCGAT and GE379 (GTGACTGGAGTTCAGACGTGTGCTCTTCCGATCTCTGCCTAACAGGAGGTGGG). Underline sequences represent target specific regions of the primers

For integration the multiplex PB vectors, 2.5 million iPS18a containing dCas9-VPR were transfected with 1 µg of pGEP150 piggyBac transposase plasmid (Barrett lab, Broad Institute) and 5 µg of pGEP163 piggyBac plasmid (Barrett lab, Broad Institute) containing 3 gRNAs targeting *XIST* via Neon electroporation under conditions described above. 24 hours after transfection, cells are treated with blasticidin at a final concentration of 2 µg/ml for 21-30 days to select for positive piggyBac integrands and allow for clearing of non-integrated plasmid. gRNA sequences for *XIST* activation were selected using CRISPR-ERA (http://crispr-era.stanford.edu/) and are as follows: gRNA1; ACCAGGAGTCACAACTTCAA. gRNA2; GGTTCAAAATTTACCCAGTA, gRNA3, TGGCCTAGAAGATTGAAAGC. We cross-referenced our selected gRNAs sequences to the FANTOM5 (http://fantom.gsc.riken.jp/) CAGE mapping database to ensure we were targeting the major predicted TSS for *XIST*. The three gRNAs driven by U6 promoter were cloned into pGEP163 via Golden Gate cloning as described (Sakuma et al., 2014). Homogeneous colonies were generated by single cell expansion with 2 µg/mL Blasticidin and gRNA expression states were confirmed by fluorescence microscopy.

Transient overexpression for *XIST* induction. The three pGEP001 (gifted from Feng Zhang) for

each gRNA (gRNA1-3) driven by the U6 promoter and SP-dCas9-VPR (Addgene, #63798) for dCas9-VPR expression driven by the EF1a promoter were co-transfected into iPS18a*XIST*i-1 via the Neon Electroporation System at 1050 mV, 30 ms, 2 pulses. After transfection, the cells were culture with 10 μM Y-27632 for 24 hours. For dox+ groups, the cells after transfection were cultured in the presence of dox for 48 hours.

Generation of single DNMT3A, single DNMT3B, and double knockout lines. HUES21 was used for the generation of all of DNMT3A/B knockout lines. Low passage (p14-16) cells were used for Figure 2 related experiments and high passage (>p34) cells were used for Figure 4 related experiments, respectively. The gRNAs previously validated were used for generation of knockout lines (Liao et al., 2015). The gRNA for DNMT3A or DNMT3B was cloned into pGEP001. The pSpCas9(BB)-2A-Puro (PX459) V2.0 (Addgene, #62988) and pGEP001 with gRNA were co-transfected via the Neon Electroporation System at 1050 mV, 30 ms, 2 pulses. At 24 hours after transfection, 1-2ug/mL puromycin was added to the culture medium for 24 hours. The Y-27632 was added to the medium after transfection until the colonies grown sufficiently for passage. The clones were subjected to H3K27me3 staining to select non-eroded clones in Figure 2.

Generation of DNMT3B inducible cell lines

The plasmids for AAVS locus targeting were obtained by Addgene (52341, 52342, and 52343). For DNMT3B coding site region with Myc-tag, which was amplified by PCR with MulI and SalI sites, was replaced into EGFP of original plasmid (52343). The sequences were confirmed by Sanger-sequence. After transfection of HUES21 DNMT3A$^{-/-}$3B$^{-/-}$ (non-eroded line) cells, the cells were grown until 80% of confluent and then subjected to puromycin (0.5-1.0 μg/mL) for 2 weeks. The efficiency of targeting and DNMT3B expression states were confirmed by immunofluorescence analysis using

anti-Myc (Cell Signaling Technology, 2276).

Genotyping. Genomic DNA was extracted using DNAeasy Blood and Tissue kit (Qiagen) and used for PCR. The amplified PCR products were sequenced and the sequence results were analyzed by TIDE (https://tide.nki.nl/) to select compound null lines (Brinkman et al., 2014). The primers used for genotyping are shown in Table S1.

RNA-FISH. The cells for RNA-FISH experiments were cultured onto coverslips. The cells were fixed with 4% paraformaldehyde in PBS- for 15 min at room temperature and then treated with 0.25% triton-X in PBS- for 20 min at room temperature. The treated samples were hybridized with gene specific probes at 37°C overnight. The hybridization buffer contains 4 mg/ml BSA, 4xSSC, 20% dextran-sulfate in nuclease free water. The gene specific DNA probes were prepared based on a previous study(Fukuda et al., 2014) by nick translation kit (Abbot) according to the manufacturer's instruction. Hybridization was conducted using a 1:1 ratio of DNA probe and hybridization buffer. After overnight hybridization, the coverslips were washed with 50% formamide containing 2x SSC at 45°C for 10 min at twice and then washed with 2xSSC containing 0.05% tween-20 at 45°C for 10 min twice. After washing, the coverslips were air-dried and mounted with VECTASHIELD with DAPI (Vectorlabs). Nikon ECIPSE Ti fluorescence microscopy and NIS-Elements AR software were used to obtain images.

For generation of *XIST* probes, plasmid containing 5-kb *XIST* exon 1 was purchased from OriGene (# SC312039). The CTD 3063K22 BAC clone was used for generating the *XACT* probe. For quantification, a minimum of 5 different colonies or fields were analyzed and the number of analyzed cells are described in each Figure. Only cells that did not overlap at interphase were used for analysis. The Fiji (https://fiji.sc/) software was used for quantification analysis and visualization.

Chromosome spreading and DNA-FISH

Sample preparation for the chromosome spreading assay was performed as previously described (Campos et al., 2009). Briefly, hPSCs were cultured in the presence of Colcemid (0.5 μg/mL) to induce metaphase. After treatment with KCl (75 mM), samples were fixed with methanol/glacial acetic acid (3:1). For the chromosome spreading assay, samples were mounted onto glass slides using VECTASHIELD (Vectorlabs) mounting medium with DAPI. For DNA-FISH, samples on the glass slides were incubated for 10 min at 85 °C with hybridization buffer containing the *XACT* probe, prepared as previously described (Fukuda et al., 2016).

Bisulfite DNA sequencing. Extracted genomic DNA was subject to bisulfite conversion using the EZ DNA methylation kit (Zymo Research). The converted DNA was used as template for PCR using EpiTaq HS (Takara). The amplified products were cloned into p-GEM t-easy vector (Promega) by TA cloning and sequenced. The results were analyzed using QUMA (http://quma.cdb.riken.jp/). The primer sequences are shown in Table S1.

qPCR. Total RNA was extracted using RNeasy plus micro kit (Qiagen) and the total RNA was converted to cDNA using iScript™ cDNA Synthesis kit (Bio-Rad). SYBR® Green Master Mix (Bio-Rad) was used for qPCR assay. The data was analyzed using $^{\Delta\Delta}$Ct methods. GAPDH was used as internal control and primers are described in Table S1.

Immunofluorescence stain. Cells were fixed with 4% paraformaldehyde in PBS- for 15 min at room temperature and then permeabilized with 0.25% triton-X in PBS- for 20 min at room temperature. The samples were incubated with 1.5% BSA in PBS- for 1 hour at room temperature. Primary antibodies

used: OCT4 (C-10, SantaCruz) and H3K27me3 (39055, Active Motif). The primary antibodies were incubated at 4°C for overnight. Secondary antibodies used: AlexaFluor 488, 555, and 647 conjugated (1:500, Invitrogen). The secondary antibodies were incubated for 1-2 hours at room temperature. After washing with PBS- at least three times, the samples were incubated with DAPI (Thermofisher Scientific) for those in plastic bottom plates. For samples cultured on glass coverslips, the samples were mounted with VECTASHIELD with DAPI. Nikon ECIPSE Ti fluorescence microscopy and NIS-Elements AR software were used to obtain images.

Immuno-FISH. Cells were fixed and permeabilized as described above. The cells were incubated with blocking buffer including RNaseOUT (1:100, Thermofisher) for 1 hour at room temperature. After wash with PBS-, the samples were incubated with ISL1 (ab109517, abcam) in blocking buffer with RNaseOUT for 1 hour. After wash with PBS-, the cells were treated with 2nd antibody in PBS- for 1 hour at room temperature. The samples were post-fixed with 4% paraformaldehyde for 10 min at room temperature. After wash with PBS-, the samples were subject to RNA-FISH.

Western Blotting. Protein was extracted using RIPA Lysis and Extraction Buffer (Thermofisher). The extracted protein was subjected to SDS-PAGE using 7.5% TGX gel (Bio-Rad) for DNMT3B (ab16049, Abcam) or 4-20% TGX Gel (Bio-Rad) for DNMT3A (2160S, Cell Signaling Technology) and GAPDH (2118, Cell Signaling Technology). Uncropped images are shown in Figure S4f.

ChIP-qPCR. Chromatin was extracted as described previously(Fukuda *et al.*, 2014). In brief, 2 million cells were collected by TryPL express (Thermofisher) and fixed with 1% formaldehyde. The cells were resuspended in SDS lysis buffer and the lysate was sonicated using S220 Focused-ultrasonicator (Covaris). The 10% of chromatin was used as input DNA collection. The chromatin was

immunoprecipitated with Protein A-beads (Veritas Life Sciences) conjugated to anti-Cas9 (Diagenode, C15310258) or rabbit IgG (Abcam, ab171870). DNA from immunoprecipitated chromatin was extracted using phenol chloroform and purified by ethanol precipitation. The DNA was analyzed by qPCR using SYBR green. The primer sequences are shown in Table S1.

RNA-sequence

Total RNA obtained from each sample was extracted using RNeasy Micro plus kit (Qiagen) and used to construct a sequencing library with the NEBNext Ultra II Directional RNA Library Prep Kit for Illumina (New England Biolabs, Ipswich, MA, USA) and NEBNext rRNA Depletion Kit (Human/Mouse/Rat) according to the manufacturer's protocols. Library quality was checked by Agilent 2200 TapeStation High Sensitivity D1000 (Agilent Technologies, Santa Clara, CA, USA). The pooled libraries of the samples were sequenced using the Illumina NextSeq 500 (Illumina, San Diego, CA) in 76-base-pair paired-end reads. Sequencing adaptors, low-quality reads, and bases were trimmed with the Trimmomatic-0.38 tool. The sequence reads were aligned to the human reference genome (hg38) using STAR 2.7.1a. Files of the gene model annotations and known transcripts were downloaded from Illumina's iGenomes website (http://support.illumina.com/sequencing/sequencing_software/igenome.html). The aligned reads were subjected to downstream analyses using the StrandNGS 3.2 software (Agilent Technologies).

Genes with ≧1 TPM in all three lines (average of biological replicates) were used for boot strap analysis. The bootstrap analysis was performed as described in previous reports (Fukuda et al., 2015; Sangrithi et al., 2017). Briefly, median X:A ratios were calculated by bootstrapping with 2000 replications and 100 expression values were randomly selected for each time from X-linked and autosomal genes using the 'sample' function of R 4.0.2 (https://www.r-project.org/). Ninety-five percent bootstrap intervals were also calculated using the 'quantile' function of R. For relative

expression analysis (Figure 3c-e), TMM normalization (Robinson and Oshlack, 2010) and genes with >1 TMM in one sample (average of biological replicates) were used. The statistics and the calculation of mean absolute deviation and hierarchical clustering analysis were conducted using R. All sequence data were deposited in GEO (GSE160454).

References

Brinkman, E.K., Chen, T., Amendola, M., and van Steensel, B. (2014). Easy quantitative assessment of genome editing by sequence trace decomposition. Nucleic Acids Res *42*, e168. 10.1093/nar/gku936.

Campos, P.B., Sartore, R.C., Abdalla, S.N., and Rehen, S.K. (2009). Chromosomal spread preparation of human embryonic stem cells for karyotyping. J Vis Exp. 10.3791/1512.

Fukuda, A., Mitani, A., Miyashita, T., Sado, T., Umezawa, A., and Akutsu, H. (2016). Maintenance of Xist Imprinting Depends on Chromatin Condensation State and Rnf12 Dosage in Mice. PLoS Genet *12*, e1006375. 10.1371/journal.pgen.1006375.

Fukuda, A., Tanino, M., Matoba, R., Umezawa, A., and Akutsu, H. (2015). Imbalance between the expression dosages of X-chromosome and autosomal genes in mammalian oocytes. Sci Rep *5*, 14101. 10.1038/srep14101.

Fukuda, A., Tomikawa, J., Miura, T., Hata, K., Nakabayashi, K., Eggan, K., Akutsu, H., and Umezawa, A. (2014). The role of maternal-specific H3K9me3 modification in establishing imprinted X-chromosome inactivation and embryogenesis in mice. Nat Commun *5*, 5464. 10.1038/ncomms6464.

Klim, J.R., Williams, L.A., Limone, F., Guerra San Juan, I., Davis-Dusenbery, B.N., Mordes, D.A., Burberry, A., Steinbaugh, M.J., Gamage, K.K., Kirchner, R., et al. (2019). ALS-implicated protein TDP-43 sustains levels of STMN2, a mediator of motor neuron growth and repair. Nat Neurosci *22*, 167-179. 10.1038/s41593-018-0300-4.

Liao, J., Karnik, R., Gu, H., Ziller, M.J., Clement, K., Tsankov, A.M., Akopian, V., Gifford, C.A., Donaghey, J., Galonska, C., et al. (2015). Targeted disruption of DNMT1, DNMT3A and DNMT3B in human embryonic stem cells. Nat Genet *47*, 469-478. 10.1038/ng.3258.

Mekhoubad, S., Bock, C., de Boer, A.S., Kiskinis, E., Meissner, A., and Eggan, K. (2012). Erosion of dosage compensation impacts human iPSC disease modeling. Cell Stem Cell *10*, 595-609. 10.1016/j.stem.2012.02.014.

Robinson, M.D., and Oshlack, A. (2010). A scaling normalization method for differential expression analysis of RNA-seq data. Genome Biol *11*, R25. 10.1186/gb-2010-11-3-r25.

Sakuma, T., Nishikawa, A., Kume, S., Chayama, K., and Yamamoto, T. (2014). Multiplex genome engineering in human cells using all-in-one CRISPR/Cas9 vector system. Sci Rep *4*, 5400. 10.1038/srep05400.

Sangrithi, M.N., Royo, H., Mahadevaiah, S.K., Ojarikre, O., Bhaw, L., Sesay, A., Peters, A.H., Stadler, M., and Turner, J.M. (2017). Non-Canonical and Sexually Dimorphic X Dosage Compensation States in the Mouse and Human Germline. Dev Cell *40*, 289-301 e283.

10.1016/j.devcel.2016.12.023.